I&EC research
Industrial & Engineering Chemistry Research

Article

Cite This: Ind. Eng. Chem. Res. 2019, 58, 8990−8995

pubs.acs.org/IECR

Manganese Oxide Nanoparticles Immobilized on Silica Nanospheres as a Highly Efficient Catalyst for Heavy Oil Oxidation

Andrey Galukhin,* Roman Nosov, Alexey Eskin, Mohammed Khelkhal, and Yuri Osin

Kazan Federal University, 18 Kremlevskaya str., Kazan 420008, Russian Federation

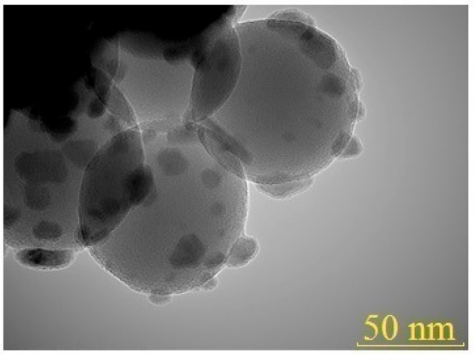

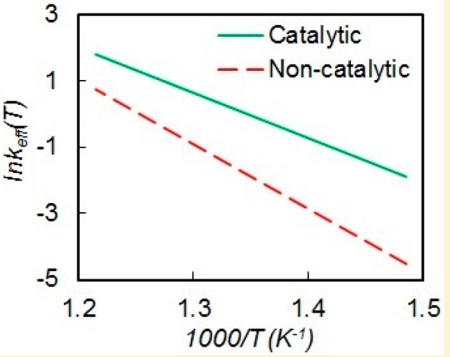

ABSTRACT: Nanoparticles have proven to be successful catalysts for oil combustion. To maximize their catalytic performance, it is necessary to provide nanoparticle aggregation stability during the combustion process. The classical approach to stabilization of nanoparticles assumes application of different stabilizers, like surfactants or polymers, attached to particles' surfaces, preventing their aggregation via steric or electrostatic repulsion. Thus, the aggregation stability of nanoparticles is determined by the thermal stability of the surfactant- or polymer-based coatings, which is not sufficient for high-temperature processes. In the current study we prepared a catalyst with high thermal stability by immobilization of 10 nm sized MnO_x nanoparticles on a surface of 70 nm silica nanospheres. The composition, morphological, and textural parameters of the catalyst were optimized via variation of synthetic conditions. The high catalytic performance of the obtained nanoparticles in heavy oil combustion was proven by evaluation of kinetic parameters of catalytic and noncatalytic processes.

1. INTRODUCTION

Shortage of conventional oil reserves combined with the growing consumption of energy resources motivates the search for alternative sources of hydrocarbons. Natural bitumen and heavy oil represent one of the largest hydrocarbon sources in the world. According to United States Geological Survey, their combined reserves are estimated to be almost 9 trillion barrels of original oil in place.[1] Development of unconventional hydrocarbon resources demands the application of special technologies. Today, in situ combustion is considered as a promising approach for extraction of heavy oil. The method implies injection of air into the oil field to oxidize part of the oil and generate heat and pressure, enhancing oil recovery. The success of the application of this method is determined by the stability of the smoldering process.[2] The use of catalytic additives promoting the oxidation process and improving properties of the extracted oil is one of the possible ways to enhance the stability of the smoldering front.[3] Many researchers' efforts were invested in finding effective catalytic systems promoting oil combustion in porous media. Currently, catalytic systems based on nanoparticles are known as the most effective catalysts for oil combustion. Compounds of different transition metals, like Cu, Fe, Ni, Ti, Zr, Ce, and Pd, in the form of nanoparticles were tested in the combustion of heavy oils and high molecular components of them.[4−9] In particular, our studies showed high catalytic activity of Mn-based catalysts in the oil oxidation process.[10,11] Detailed investigation of the transformation of the active phase of the catalyst by X-ray powder diffraction and electron paramagnetic resonance techniques allowed us to reveal some mechanistic insights into catalytic oil oxidation.[10] In general, catalysts based on platinum group metals and rare-earth elements possess superior catalytic activity toward organic matter oxidation; however, the high prices of these metals hinder their application for heavy oil production, and use of transition metals of the fourth period for that purpose looks more reasonable.

The variation of morphological parameters (size and shape) of nanoparticles is commonly used to achieve their high catalytic performance. It is well-known that decrease in particle size leads to increase in their specific surface area, which favors the kinetics of heterogeneous reactions.[12] On the other hand, decrease of particle size results in their aggregation instability, which may dramatically affect catalytic performance.[13,14] Usually, different stabilizers, like surfactants[15,16] or poly-

Received: January 9, 2019
Revised: April 30, 2019
Accepted: May 7, 2019
Published: May 7, 2019

DOI: 10.1021/acs.iecr.9b00080
Ind. Eng. Chem. Res. 2019, 58, 8990−8995

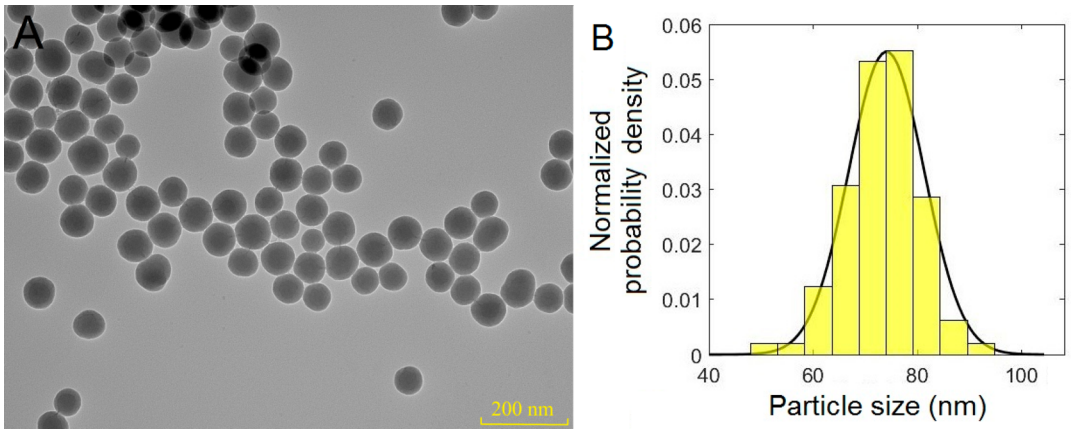

Figure 1. TEM image of synthesized SNP (A) and particle size distribution (B).

mers[17,18] attached to particles' surfaces, are used to prevent their aggregation via steric or electrostatic repulsion. However, because of the low thermal stability of such surfactant- and polymer-based coatings, the aggregation stability of nanocatalysts worsens with increasing temperature, which may significantly decrease their catalytic activity in high-temperature processes.

The current study is the next stage of our investigations of Mn-based catalysts in heavy oil oxidation processes. In order to further increase their catalytic activity, we prepared nanosized MnO_x particles, the aggregation stability of which was provided by their deposition on a surface of silica nanoparticles. The application of such a nanosupport allowed us to overcome the high-temperature stability issue.

2. MATERIALS AND METHODS

2.1. Materials. Ammonium hydroxide solution (28−30% of NH_3, Sigma-Aldrich), tetraethoxysilane (99.9%, Sigma-Aldrich), $Mn(NO_3)_2{\cdot}4H_2O$ (analytical grade, Acros Organics), methanol (99.9%, Sigma-Aldrich), and ethanol (96%, RFK ltd.) were purchased and used without purification. Ashalcha heavy crude oil (Russia) was used in this research for catalytic combustion study. The detailed description of the heavy oil physical properties, as well as its composition, can be found in our previous study.[19]

2.2. Synthesis of Silica Nanospheres. Silica nanospheres were synthesized by a modified Stober method.[20] A 500 mL portion of ethanol−methanol mixture (1:1 ratio) in a round-bottom flask equipped with a magnetic stirrer was heated to 55 °C. Then, 17.7 g of TEOS, 52.5 mL of ammonium hydroxide solution, and 8.5 mL of deionized water were subsequently added to the reaction mixture. The reaction was carried at 55 °C for 12 h under vigorous stirring. Silica nanospheres were isolated by centrifugation (8000 rotations per minute) and washed with ethanol. The dried silica nanospheres were then calcined at 600 °C for 24 h. The final yield of silica nanospheres was 4.1 g (80%).

2.3. Preparation of Mn-Based Supported Catalyst Samples. A suspension of the silica nanoparticles in an appropriate amount of 2 M manganese(II) nitrate solution was made; the solvent was then evaporated in rotary evaporator, and the resulting precatalysts were calcined at a temperature of 600 °C for 8 h. Samples with manganese content of 2.3, 4.8, 8.7, and 10.9% are denoted subsequently as SNP-Mn1, SNP-Mn2, SNP-Mn3, and SNP-Mn4, respectively.

2.4. X-ray Powder Diffraction. X-ray powder diffraction (XRPD) measurements were carried out with a MiniFlex 600 diffractometer (Rigaku).

2.5. Thermal Analysis. All calorimetric measurements were carried out using an STA 449 F1 Jupiter (Netzsch) thermoanalyzer in a temperature range of 50−600 °C. The measurements were performed in the atmosphere of flowing air (50 mL min^{-1}) in open 85 μL corundum crucibles at linear heating rates of 5, 10, 15, and 20 °C min^{-1}. The sample mass for each run was ∼10 mg. Samples for differential scanning calorimetry were made by mixing the oil (10 wt %) with the catalyst (10 wt %) and the fractioned quartz sand (43−64 μm, 80 wt %). Noncatalytic studies were performed with a sample made of oil (10 wt %) and the same quartz sand (90 wt %).

2.6. Transmission Electron Microscopy and Energy-Dispersive X-ray Spectroscopy. Transmission electron microscopy (TEM) images were obtained with a transmission electron microscope (Hitachi HT7700 Excellence). Energy dispersive spectrometer AZtec X-MAX was used for the elemental analysis of all samples.

2.7. Specific Surface Area Measurements. Specific surface area (SSA) values of synthesized catalysts were calculated with the Brunauer−Emmett−Teller (BET) equation applied to nitrogen adsorption data (77 K, relative pressure range of 0.05−0.30) measured by an ASAP 2020 MP instrument (Micromeritics).

3. RESULTS AND DISCUSSION

Among the aforementioned transition metals, manganese deserves special attention because it is widely applied for catalysis in processes of full[21,22] and partial[23,24] oxidation of organic compounds, which combined with low toxicity and availability makes it excellent catalytic material for acceleration of heavy oil combustion in porous media. Our previous studies[10,11] showed Mn-based catalysts demonstrate high catalytic activity in heavy oil oxidation processes. We also investigated the catalytic cycle of the Mn(II)-based catalyst's precursor and showed that it includes transitions of Mn between +2 and +3 oxidation states.[10]

A modified Stober technique[20] was used for production of silica nanoparticles. The technique is based on hydrolysis of tetraethoxysilane in an alcohol−water mixture catalyzed by ammonia. Variation of synthesis conditions (temperature and concentrations of the reactants) allows control of the size and polydispersity of produced nanoparticles.[25,26] TEM was

DOI: 10.1021/acs.iecr.9b00080
Ind. Eng. Chem. Res. 2019, 58, 8990−8995

applied to examine the morphological parameters of the synthesized silica nanoparticles (Figure 1A). TEM images show most of the nanoparticles possess a spherical shape, with the average size of spheres of 74 ± 7 nm. Particle size distribution is presented in Figure 1B. Obtained SNPs were used as a support for nanosized particles of the Mn-based active phase.

We used impregnation of the obtained SNP by $Mn(NO_3)_2$ solution followed by high-temperature calcination to prepare Mn-based supported catalysts. High-temperature calcination was used to decompose the initial salt into MnO_x nanoparticles and convert Mn(II) into higher oxidation states. XRPD analysis of the obtained samples revealed the presence of Mn_2O_3 and Mn_5O_8 phases. Figure 2 shows that increase in

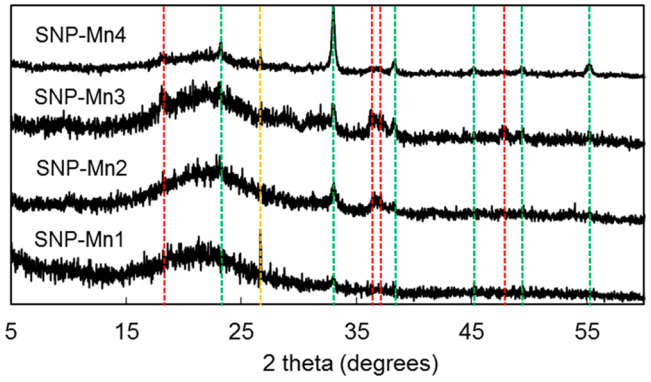

Figure 2. XRPD analysis of synthesized supported catalysts. Colored dashed lines designate the following phases: quartz (orange), bixbyite Mn_2O_3 (green), and Mn_5O_8 (red).

content of manganese in calcined samples results in a decrease of the Mn_5O_8/Mn_2O_3 phase ratio. It should be noted that the presence of Mn_5O_8 in MnO_x oxidation catalysts increases their activity in hydrocarbon oxidation because of increased oxygen mobility in the Mn_5O_8 phase.[27] Thus, catalysts with higher content of Mn_5O_8 phase are more promising in heavy oil combustion processes.

Nitrogen adsorption measurements were used for determination of the specific surface area of the obtained supported catalysts. Typical adsorption isotherm as well as BET surface area plots of Mn-based supported catalyst sample are presented in Figure 3.

The results of measurements as well as the content of Mn for all samples determined by energy dispersive X-ray (EDX) spectroscopy are grouped in Table 1.

One can see (Table 1) that increase of the Mn content higher than 5 wt % leads to significant decrease of surface area of the catalysts. This might be caused by increase in size of the crystallites of the active phase during calcination stage.

This suggestion was proven by transmission electron microscopy (Figure 4). Figure 4A shows the SNP-Mn1 (2.3 wt % of Mn) sample contains approximately 10 nm sized nanoparticles dispersed on silica spheres. Increase of Mn content in the SNP-Mn2 sample yields an increase of the amount of the manganese oxide nanoparticles per unit of silica surface; the size of the particles remains the same (Figure 4B). Further increase of Mn content results in significant increase in the size of crystallites of the active phase (Figure 4C,D).

Thus, among all obtained catalysts, the SNP-Mn2 sample was chosen for catalytic testing in heavy oil combustion

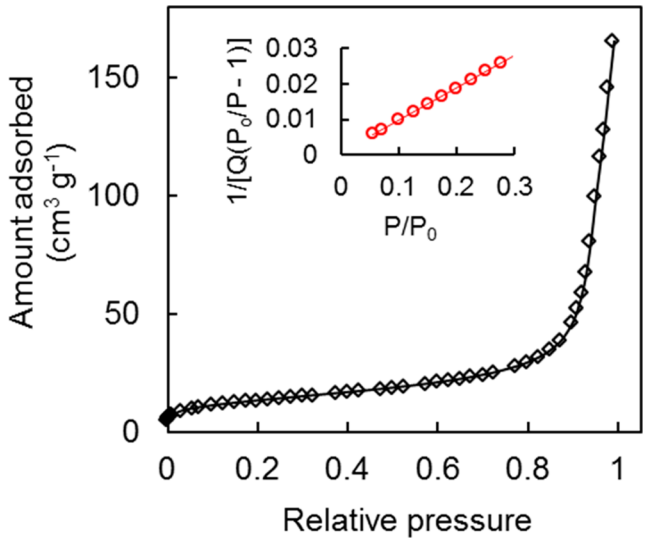

Figure 3. Nitrogen adsorption isotherm at 77 K and BET plots (inset) of SNP-Mn2.

Table 1. Mn Content and Specific Surface Area of Obtained Catalyst Samples

sample	Mn content by EDX (wt %)	SSA ($m^2 \cdot g^{-1}$)
SNP	0.0	46.4 ± 0.4
SNP-Mn1	2.3	46.9 ± 0.4
SNP-Mn2	4.8	47.4 ± 0.3
SNP-Mn3	8.7	38.9 ± 0.3
SNP-Mn4	10.9	36.8 ± 0.3

processes because of the high value of the Mn_5O_8/Mn_2O_3 ratio (Figure 2), highest SSA value (Table 1), and small size of the active phase crystallites (Figure 4).

Because the heavy oil combustion is a strongly exothermic process, it is convenient to follow it by means of differential scanning calorimetry (DSC). Major advantages of the application of DSC in such studies are small sample sizes, accuracy, and small measurement times. Figure 5 shows the presence of two overlapped exothermic signals in the heat flow curves for both noncatalytic and catalytic processes, corresponding to low (LTO) and high-temperature oxidation (HTO) processes. LTO includes numbers of reactions yielding oxygen-containing organic compounds (peroxides, alcohols, and carbonyl compounds) and yielding small amounts of carbon mono- and dioxide. The coke combustion producing carbon oxides and water is believed to be the key reaction of HTO.[28−30] Table 2 summarizes reaction intervals and peak temperatures of the low- and high-temperature oxidation reactions for both noncatalytic and catalytic processes. It can be clearly seen that the addition of catalyst shifts HTO's heat flow signal to lower temperatures.

Figure 6 shows the differences between pairs of T_p values corresponding to the same heating rates (β) for noncatalytic and catalytic processes for both low- and high-temperature oxidation. From Figure 6, significant differences between noncatalytic and catalytic processes for HTO can clearly be seen; at the same time, the catalyst shows negligible influence on LTO processes.

We applied the Kissinger method[31] to calculate kinetic parameters of oil oxidation. This method relates the variation of peak temperatures (T_p) of the heat flow signal obtained at

DOI: 10.1021/acs.iecr.9b00080
Ind. Eng. Chem. Res. 2019, 58, 8990−8995

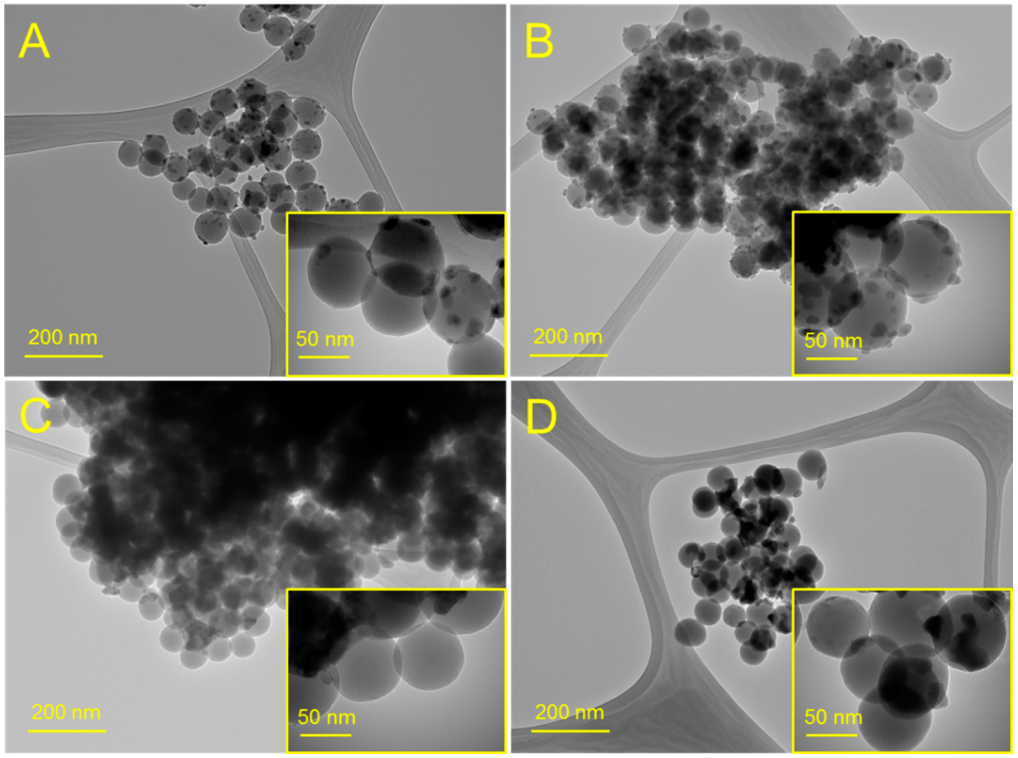

Figure 4. TEM images of SNP-Mn1 (A), SNP-Mn2 (B), SNP-Mn3 (C), and SNP-Mn4 (D). Scale bars are 200 and 50 nm (inset).

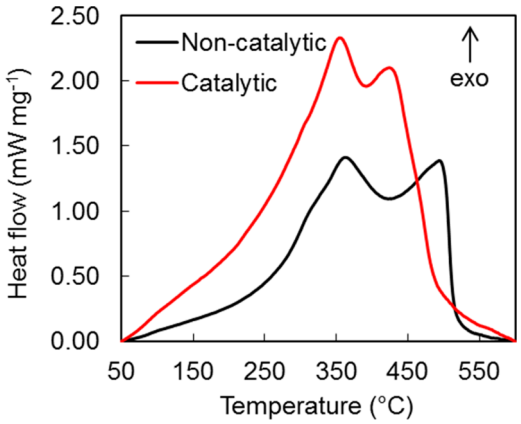

Figure 5. Heat flow curves for noncatalytic and catalytic oil oxidation at 10 °C min^{-1}.

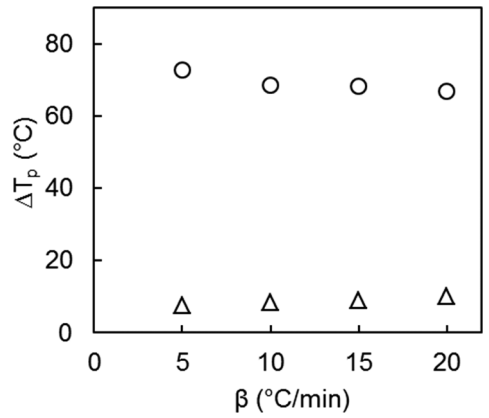

Figure 6. Differences between the peak temperatures (ΔT_p) of noncatalytic and catalytic heavy oil combustion for LTO (triangles) and HTO (circles) at different heating rates.

Table 2. Reaction Intervals and Peak Temperatures of Noncatalytic and Catalytic Heavy Oil Combustion

		noncatalytic		catalytic	
type of oxidation	β (°C min^{-1})	reaction interval (°C)	T_p (°C)	reaction interval (°C)	T_p (°C)
LTO	5	248–380	343	256–417	336
	10	276–409	364	298–436	356
	15	280–422	376	311–438	367
	20	291–426	386	329–449	376
HTO	5	433–489	473	395–430	400
	10	439–514	494	414–456	425
	15	444–528	502	427–480	434
	20	450–538	512	439–492	445

different heating rates (β) to values of Arrhenius parameters (E and A):

$$\ln\left(\frac{\beta}{T_p^2}\right) = -\frac{E_a}{R}\frac{1}{T_p} + \ln\left(\frac{AR}{E_a}\right) \quad (1)$$

We chose the Kissinger method over a number of other methods[32−35] because the complexity of the obtained heat flow curves hinders the choice of a proper baseline. Because the peak temperature values needed for calculations are practically independent of the baseline selection, this method is a reasonable alternative to other methods. Figure 7 shows $\ln(\beta/T^2)$ vs $1/T$ plots for the studied reactions; the calculated kinetic parameters are presented in Table 3.

One can see that in the case of LTO, both catalytic and noncatalytic reactions possess similar Arrhenius parameters (Table 3); therefore, their reaction rates should also be similar. The situation is not nearly the same for HTO: compared to the

DOI: 10.1021/acs.iecr.9b00080
Ind. Eng. Chem. Res. 2019, 58, 8990−8995

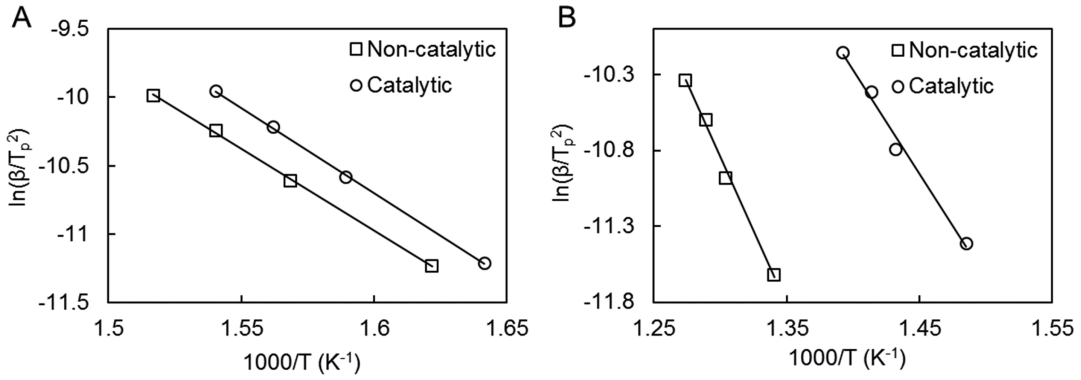

Figure 7. $\ln(\beta/T^2)$ vs $1/T$ plots for catalytic and noncatalytic low-temperature (A) and high-temperature (B) oxidation.

Table 3. Arrhenius Parameters of Combustion Processes

	noncatalytic		catalytic	
	LTO	HTO	LTO	HTO
E_a (kJ/mol)	100.0 ± 1.8	161.8 ± 8.3	104.0 ± 1.7	113.5 ± 8.4
ln A (A in min^{-1})	17.7	24.4	18.7	18.4

noncatalytic reaction, the respective activation energy value is significantly lower for the catalytic process, suggesting that the reaction should proceed faster. On the other hand, catalytic HTO shows a lower pre-exponential factor A value; therefore, the catalytic reaction should be slower than that of noncatalytic oxidation.

To demonstrate the overall effect of these parameters on reaction kinetics, we evaluated the rate constant (k) as

$$\ln k = \ln A - E_a/RT \quad (2)$$

Figure 8 shows negligible difference between rate constants of noncatalytic and catalytic combustion for LTO (Figure 8A), while in the case of HTO (Figure 8B), the catalytic process proceeds significantly faster. Because the results in $k(T)$ are significantly larger for the catalytic reaction, we can conclude that decrease in its activation energy makes the major contribution to enhanced reactivity of oil in catalytic combustion.

These results are consistent with previously obtained ones for submicrosized manganese oxide particles.[11] We explain the insignificant effect of manganese oxide nanoparticles on LTO as resulting from strong adsorption of resins and asphaltenes, as the most polar components of oil containing significant amount of heteroatoms, on the polar surface of MnO_x nanoparticles. This explanation looks reasonable because the strong affinity of asphaltenes to surfaces of basic, acidic, and amphoteric metal oxides is well-known.[36,37] The adsorption of polar substances on a surface of a catalyst's active phase may decrease its availability to hydrocarbon participating in LTO and thus decrease activity of catalyst in low-temperature oxidation processes.

4. CONCLUSIONS

We synthesized a catalyst for heavy oil oxidation based on nanosized MnO_x particles, the aggregation stability of which is provided by their immobilization on silica nanospheres. The composition of the catalyst was optimized to achieve appropriate morphological parameters of the active phase. The composition, morphological, and textural parameters of the catalyst were studied in depth by TEM, nitrogen adsorption measurements, X-ray phase diffraction analysis, and energy dispersive X-ray analysis. The investigation of heavy oil combustion in the absence and presence of the synthesized catalyst by differential scanning calorimetry revealed its high catalytic performance. Analysis of the kinetics made by the Kissinger method shows that the catalyst influences mostly the high-temperature oxidation process.

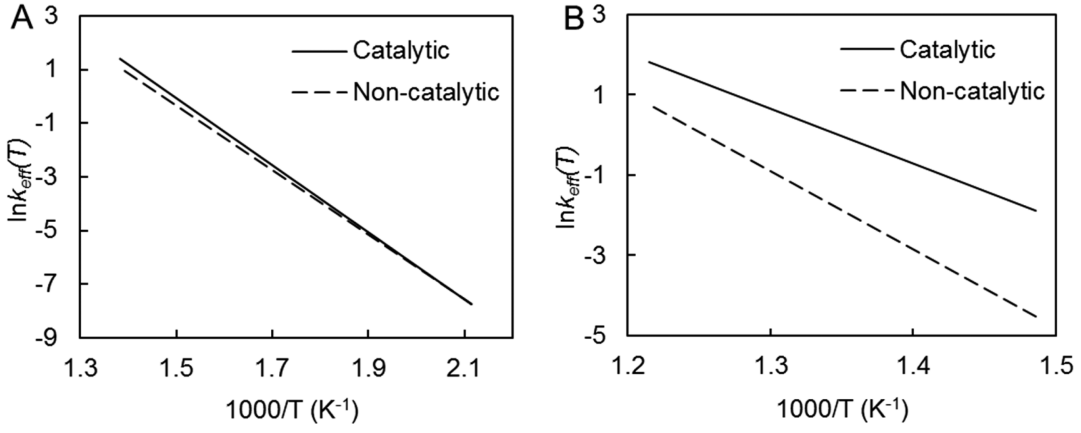

Figure 8. Variation of effective rate constants with temperature for catalytic and noncatalytic low-temperature (A) and high-temperature (B) oxidation.

DOI: 10.1021/acs.iecr.9b00080
Ind. Eng. Chem. Res. 2019, 58, 8990−8995

AUTHOR INFORMATION

Corresponding Author

*E-mail: and_galuhin@mail.ru.

ORCID

Andrey Galukhin: 0000-0003-3077-3816

Funding

This research was conducted with support of the Russian Science Foundation (Project No. 17-73-10350).

Notes

The authors declare no competing financial interest.

REFERENCES

(1) Meyer, R. F.; Attanasi, E. D.; Freeman, P. A. *Heavy oil and natural bitumen resources in geological basins of the world: U.S. geological survey open report.*; U.S. Geological Survey, Reston, VA, 2007; pp 17.

(2) Baud, G.; Salvador, S.; Debenest, G.; Thovert, J.-F. New Granular Model Medium To Investigate Smoldering Fronts Propagation—Experiments. *Energy Fuels* **2015**, *29*, 6780.

(3) Abuhesa, M. B.; Hughes, R. Comparison of Conventional and Catalytic in Situ Combustion Processes for Oil Recovery. *Energy Fuels* **2009**, *23*, 186.

(4) Amanam, U.; Kovscek, A. Analysis of the effects of copper nanoparticles on in-situ combustion of extra heavy-crude oil. *J. Pet. Sci. Eng.* **2017**, *152*, 406.

(5) Nassar, N. N.; Hassan, A.; Carbognani, L.; Lopez-Linares, F.; Pereira-Almao, P. Iron oxide nanoparticles for rapid adsorption and enhanced catalytic oxidation of thermally cracked asphaltenes. *Fuel* **2012**, *95*, 257.

(6) Marei, N. N.; Nassar, N. N.; Vitale, G.; Hassan, A.; Pérez Zurita, M. J. Effects of the size of NiO nanoparticles on the catalytic oxidation of Quinolin-65 as an asphaltene model compound. *Fuel* **2017**, *207*, 423.

(7) Marei, N. N.; Nassar, N. N.; Hmoudah, M.; El-Qanni, A.; Vitale, G.; Hassan, A. Nanosize effects of NiO nanosorbcats on adsorption and catalytic thermo oxidative decomposition of vacuum residue asphaltenes. *Can. J. Chem. Eng.* **2017**, *95*, 1864.

(8) Nassar, N. N.; Hassan, A.; Vitale, G. Comparing kinetics and mechanism of adsorption and thermo-oxidative decomposition of Athabasca asphaltenes onto TiO2, ZrO2, and CeO2 nanoparticles. *Appl. Catal., A* **2014**, *484*, 161.

(9) Montoya, T.; Argel, B. L.; Nassar, N. N.; Franco, C. A.; Cortés, F. B. Kinetics and mechanisms of the catalytic thermal cracking of asphaltenes adsorbed on supported nanoparticles. *Pet. Sci.* **2016**, *13*, 561.

(10) Galukhin, A.; Khelkhal, M. A.; Gerasimov, A.; Biktagirov, T.; Gafurov, M.; Rodionov, A.; Orlinskii, S. Mn-Catalyzed Oxidation of Heavy Oil in Porous Media: Kinetics and Some Aspects of the Mechanism. *Energy Fuels* **2016**, *30*, 7731.

(11) Galukhin, A. V.; Khelkhal, M. A.; Eskin, A. V.; Osin, Y. N. Catalytic Combustion of Heavy Oil in the Presence of Manganese-Based Submicroparticles in a Quartz Porous Medium. *Energy Fuels* **2017**, *31*, 11253.

(12) Atkins, P.; De Paula, J. *Physical Chemistry*, 10th ed.; W.H. Freeman: New York, 2014.

(13) Newton, J.; Preece, J.; Pollet, B. Control of nanoparticle aggregation in PEMFCs using surfactants. *Int. J. Low-Carbon Technol.* **2012**, *7*, 38.

(14) Jiang, Zh.; Liu, Ch.; Sun, L. Catalytic Properties of Silver Nanoparticles Supported on Silica Spheres. *J. Phys. Chem. B* **2005**, *109*, 1730.

(15) Li, N.; Zhang, X.; Chen, Sh.; Hou, X. Synthesis and characterization of CdS nanoparticles in the presence of oleic acid as solvent and stabilizer. *J. Phys. Chem. Solids* **2011**, *72*, 1195.

(16) Xu, Z.; Shen, Ch.; Hou, Y.; Gao, H.; Sun, Sh. Oleylamine as Both Reducing Agent and Stabilizer in a Facile Synthesis of Magnetite Nanoparticles. *Chem. Mater.* **2009**, *21*, 1778.

(17) Rahme, K.; Oberdisse, J.; Schweins, R.; Gaillard, C.; Marty, J.-D.; Mingotaud, C.; Gauffre, F. Pluronics-Stabilized Gold Nanoparticles: Investigation of the Structure of the Polymer−Particle Hybrid. *ChemPhysChem* **2008**, *9*, 2230.

(18) Holden, M.; Nick, K.; Hall, M.; Milligan, J.; Chen, Q.; Perry, C. Synthesis and catalytic activity of pluronic stabilized silver−gold bimetallic nanoparticles. *RSC Adv.* **2014**, *4*, 52279.

(19) Galukhin, A.; Erokhin, A.; Osin, Y.; Nurgaliev, D. Catalytic Aquathermolysis of Heavy Oil with Iron Tris(acetylacetonate): Changes of Heavy Oil Composition and in Situ Formation of Magnetic Nanoparticles. *Energy Fuels* **2015**, *29*, 4768.

(20) Huang, Y.; Pemberton, J. E. Synthesis of uniform, spherical sub-100nm silica particles using a conceptual modification of the classic LaMer model. *Colloids Surf., A* **2010**, *360*, 175.

(21) Piumetti, M.; Fino, D.; Russo, N. Mesoporous manganese oxides prepared by solution combustion synthesis as catalysts for the total oxidation of VOCs. *Appl. Catal., B* **2015**, *163*, 277.

(22) Santos, V.; Pereira, M.; Orfao, J.; Figueiredo, J. L. The role of lattice oxygen on the activity of manganese oxides towards the oxidation of volatile organic compounds. *Appl. Catal., B* **2010**, *99*, 353.

(23) Kuwahara, Y.; Yoshimura, Y.; Yamashita, H. In situ-created Mn(III) complexes active for liquid-phase oxidation of alkylaromatics to aromatic ketones with molecular oxygen. *Catal. Sci. Technol.* **2016**, *6*, 442.

(24) Huang, G.; Luo, J.; Deng, C. C.; Guo, Y. A.; Zhao, S. K.; Zhou, H.; Wei, S. Catalytic oxidation of toluene with molecular oxygen over manganese tetraphenylporphyrin supported on chitosan. *Appl. Catal., A* **2008**, *338*, 83.

(25) Giesche, H. Synthesis of Monodispersed Silica Powders I. Particle Properties and Reaction Kinetics. *J. Eur. Ceram. Soc.* **1994**, *14*, 189.

(26) Giesche, H. Synthesis of monodispersed silica powders II. Controlled growth reaction and continuous production process. *J. Eur. Ceram. Soc.* **1994**, *14*, 205.

(27) Deng, Q.-F.; Ren, T.-Zh.; Yuan, Zh.-Y. Mesoporous manganese oxide nanoparticles for the catalytic total oxidation of toluene. *React. Kinet., Mech. Catal.* **2013**, *108*, 507.

(28) Sarathi, P. *In-situ Combustion Handbook: Principles and Practices.*; National Technology Information Service: Bartlesville, OK, 1999; pp 42.

(29) Bousaid, I.; Ramey, H. Oxidation of crude oil in porous media. *SPEJ, Soc. Pet. Eng. J.* **1968**, *8* (June), 137.

(30) Fassihi, M. R.; Brigham, W. E.; Ramey, H. J. J. Reaction Kinetics of In-Situ Combustion: Part 1-Observations. *SPEJ, Soc. Pet. Eng. J.* **1984**, *24* (August), 399.

(31) Kissinger, H. Variation of Peak Temperature with Heating Rate in Differential Thermal Analysis. *J. Res. Natl. Bur. Stand.* **1956**, *57* (4), 217.

(32) Vyazovkin, S.; Burnham, A. K.; Criado, J. M.; Pérez-Maqueda, L.; Popescu, C.; Sbirrazzuoli, N. ICTAC Kinetics Committee Recommendations for Performing Kinetic Computations on Thermal Analysis Data. *Thermochim. Acta* **2011**, *520*, 1.

(33) Ozawa, T. A New Method of Analyzing Thermogravimetric Data. *Bull. Chem. Soc. Jpn.* **1965**, *38* (11), 1881.

(34) Vyazovkin, S.; Dollimore, D. Linear and Nonlinear Procedures in Isoconversional Computations of the Activation Energy of Nonisothermal Reactions in Solids. *J. Chem. Inf. Comp. Sci.* **1996**, *36*, 42.

(35) Friedman, H. Kinetics of thermal degradation of char forming plastics from thermogravimetry. Application to a phenolic plastic. *J. Polym. Sci., Part C: Polym. Symp.* **1964**, *6*, 183.

(36) Nassar, N.; Hassan, A.; Pereira-Almao, P. Metal Oxide Nanoparticles for Asphaltene Adsorption and Oxidation. *Energy Fuels* **2011**, *25*, 1017.

(37) Hosseinpour, N.; Khodadadi, A.; Bahramian, A.; Mortazavi, Y. Asphaltene Adsorption onto Acidic/Basic Metal Oxide Nanoparticles toward in Situ Upgrading of Reservoir Oils by Nanotechnology. *Langmuir* **2013**, *29*, 14135.

DOI: 10.1021/acs.iecr.9b00080
Ind. Eng. Chem. Res. 2019, 58, 8990−8995